

A Persistent Spatial Semantic Representation for High-level Natural Language Instruction Execution

Valts Blukis^{1,2}, Chris Paxton¹, Dieter Fox^{1,3}, Animesh Garg^{1,4}, Yoav Artzi²

¹NVIDIA

²Cornell University

³University of Washington

⁴University of Toronto, Vector Institute

Abstract:

Natural language provides an accessible and expressive interface to specify long-term tasks for robotic agents. However, non-experts are likely to specify such tasks with high-level instructions, which abstract over specific robot actions through several layers of abstraction. We propose that key to bridging this gap between language and robot actions over long execution horizons are persistent representations. We propose a persistent spatial semantic representation method, and show how it enables building an agent that performs hierarchical reasoning to effectively execute long-term tasks. We evaluate our approach on the ALFRED benchmark and achieve state-of-the-art results, despite completely avoiding the commonly used step-by-step instructions. <https://hlsm-alfred.github.io/>

Keywords: vision and language, spatial representations

1 Introduction

Mobile manipulation in a home environment requires addressing multiple challenges, including making long-term inference about actions to perform, where to explore, and which manipulations are necessary to enable others in the future. In addition to reasoning, robot agents also require an accessible, yet sufficiently expressive interface to specify the full diversity of possible tasks. Natural Language provides an intuitive mechanism for task specification, and coupled with advances in automated language understanding, is increasingly applied to embodied agents [e.g., 1?–9].

However, robust reasoning about manipulation goals from unrestricted natural language instruction has a variety of open challenges. For example, consider a object retrieval task in a home (Figure 1) with the instruction *secure two discs in a bedroom safe*. The robot must first locate the specific *safe* in the *bedroom*. It then needs to distribute the actions entailed by *secure* to two separate objects (*two discs*), each requiring a distinct sequence of actions, but targeting the same *safe*. It is also required to map between *secure* and its action space. In parallel, the robot must still address core mobile manipulation challenges, and often can only identify what actions are required as it observes and manipulates the world (e.g., the *safe* only needs to be opened if closed).

In this paper, we study the problem of learning to map high-level natural language instructions to low-level mobile manipulation actions in an interactive 3D environment [10] without step-by-step low-level instructions. Existing work largely studies language tightly aligned to the robot actions, either using single-sentence instructions [e.g., 1, 2, 5, 9] or sequences of instructions [11–13]. In contrast, we focus on high-level instructions, which require implicit reasoning across layers of abstraction to generate actions not explicitly specified in the instruction. Key to our approach is hierarchical reasoning about high-level subgoals and their underlying low-level motion and manipulation capabilities. In our example (Figure 1), the sequence of subgoals is ⟨pick up a CD, open the safe, put the CD in the safe, ...⟩ and each is aligned with the corresponding actions the system takes to accomplish it. Generating the sequences of subgoals and actions requires global and consistent reasoning about the world state, for example to repeatedly return to the same *safe*.

We propose to construct and continually update a spatial semantic representation of the world from sequential robot observations, as it explores and acts (Figure 2). This persistent representation allows to select subgoals that use previously observed objects currently outside of the agent’s view, or to decide about needed exploration. Similar to widely used map representations [14], we retain the spatial properties of the environment, allowing the robot to effectively navigate and reason about the relations between objects, as expressed in the language or as required to accomplish its task. We

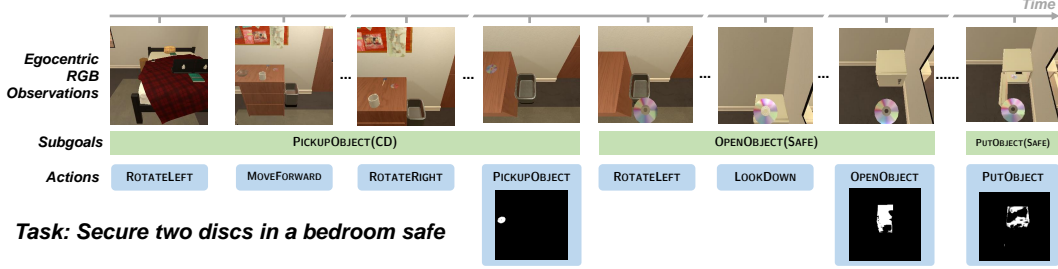
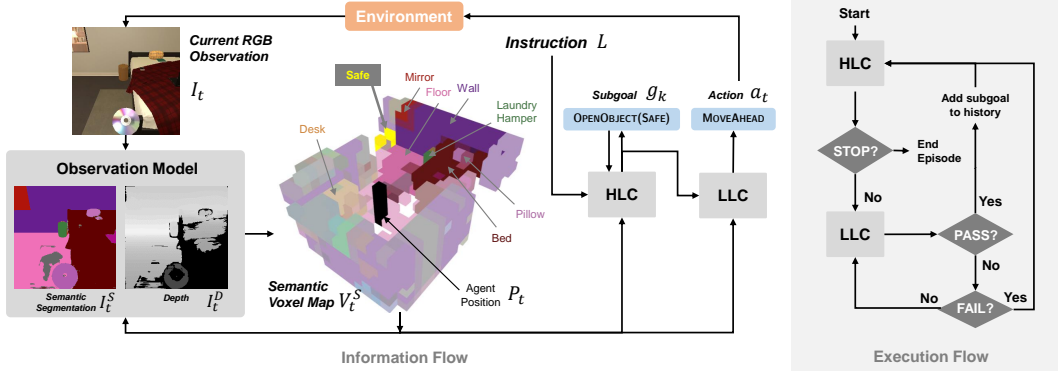


Figure 1: Illustration of the task and our hierarchical formulation. The agent receives a high-level goal specified in a natural language instruction. The goal of the agent is to map a sequence of RGB images to a sequence of navigation and manipulation actions that achieve the specified goal.



show that our spatial representation is particularly suitable for hierarchical reasoning, which alternates between selecting the next subgoal and generating the actions to accomplish it, and propose a Hierarchical Language-conditioned Spatial Model (HLSM) design.

We evaluate our approach on the ALFRED [10] benchmark, showing the benefit of combining our spatial representation with hierarchical reasoning, allowing us to achieve state-of-the-art results without low-level instructions used by previous work [11–13]. This paper makes three key contributions: (a) the first demonstration of a modular representation learning approach for the problem of mapping high-level natural language task descriptions to actions in a 3D environment; (b) a method for utilizing a spatial semantic representation within a hierarchical model for solving mobile manipulation tasks; and (c) state-of-the-art performance on the ALFRED benchmark with only high-level instructions, instead of the more commonly used step-by-step instructions.

2 Related Work

Natural language has been extensively studied in robotics research, including with focus on instruction [1, 15], reference resolution [16], question generation [17], and dialogue [4, 18]. Most work in this area has considered either synthetic instructions of relatively simple goals [7, 19–21], or natural language instructions where all intermediate steps are explained in detail [5, 10, 22? –27]. In contrast, we focus on high-level instructions, which are more likely in home environments [28].

Representation of world state, action history, and language semantics plays a central role in robot systems and their algorithm design. Symbolic representations have been extensively studied for instruction following agents [1–4, 28–35]. While they simplify the symbol grounding problem, they are laborious to scale to new environments and complex language. Representation learning presents an alternative by learning to map raw observations and language directly to actions [5, 8, 9, 22? ?

. World state and language semantics are typically represented with vectors [22] or by memorizing past observations [8, 12]. Modelling improvements have enabled representation learning approaches to achieve good performance on complex language-conditioned navigation tasks [7, 9, 22, 25?, 26], but this success has not yet translated to mobile manipulation [10, 36, 37]. We propose integrating a spatial representation in the form of a semantic voxel map within a hierarchical representation learning system. Semantic 2D maps have been successfully used in grounded language navigation tasks [7, 8, 38, 39]. We show that 3D semantic maps effectively facilitate following high-level natural language mobile manipulation instructions as well.

3 Problem Definition

Let \mathcal{A} be the set of agent actions, and \mathcal{S} the set of world states. Given a natural language instruction L and an initial state $s_0 \in \mathcal{S}$, the agent’s goal is to generate an execution $\Xi = \langle s_0, a_0, s_1, a_1, \dots, s_T, a_T \rangle$, where $a_t \in \mathcal{A}$ is an action taken by the agent at time t , $s_t \in \mathcal{S}$ is the state before taking a_t , and $s_{t+1} = \mathcal{T}(s_t, a_t)$ under environment dynamics $\mathcal{T} : \mathcal{S} \rightarrow \mathcal{S}$. The state s_t is defined by the environment layout and the poses and states of all objects and the agent. The agent does not have access to the state s_t , but only to an observation o_t . An observation $o_t = (I_t, P_t, v_t^S, L)$ includes a first-person RGB camera image I_t , the agent’s pose P_t , a one-hot encoding of the object class the agent is holding v_t^S , and the instruction L .¹ The task is considered successful if all goal-conditions corresponding to the task L are true at the final state s_T . Partial success is measured as the fraction of goal-conditions that have been achieved.

The ALFRED dataset includes sets of seen and unseen environments. The set of actions $\mathcal{A} = \mathcal{A}_{\text{nav}} \cup \mathcal{A}_{\text{int}}$ includes parameter-free navigation actions $\mathcal{A}_{\text{nav}} = \{\text{MOVEAHEAD}, \text{ROTATELEFT}, \text{ROTATERIGHT}\}$ and interaction actions $\mathcal{A}_{\text{int}} = \{\text{PICKUP}, \text{PUT}, \text{TOGGLEON}, \text{TOGGLEOFF}, \text{OPEN}, \text{CLOSE}, \text{SLICE}\}$ parameterized by a binary mask that identifies the argument of the interaction in the agent’s current first-person view.

4 Hierarchical Model with a Persistent Spatial Semantic Representation

We model the agent behavior with a policy π that maps an instruction L and the observation o_t at time t to an action a_t . The policy π is made of an *observation model* F and two controllers: a *high-level controller* π^H and a *low-level controller* π^L . The policy maintains a *spatial state representation* \hat{s}_t that captures its cumulative knowledge of the world at time t . Figure 2 illustrates the policy.

The high-level controller π^H computes a probability over *subgoals*. A subgoal g is a tuple $(\text{type}, \arg^C, \arg^M)$, where $\text{type} \in \mathcal{A}_{\text{int}}$ is an interaction type (e.g., OPEN, PICKUP), \arg^C is the semantic class of the interaction argument (e.g., SAFE, CD), and \arg^M is a 3D mask identifying the location of the argument instance. In ALFRED, each interaction action in the set \mathcal{A}_{int} corresponds to a subgoal type. When predicting the k -th subgoal at time t , π^H considers the instruction L , the current state representation \hat{s}_t , and the sequence of past subgoals $\langle g_i \rangle_{i < k}$. During inference, we sample from π^H . Unlike $\arg \max$, sampling allows the agent to re-try different subgoals if one fails (e.g., if a MUG was not found, pick up a CUP).

The low-level controller π^L is given the subgoal g_k as its goal specification at time t . At every timestep $j > t$, π^L maps the state representation \hat{s}_j and subgoal g_k to an action a_j , until it outputs one of the stop actions: a_{PASS} or a_{FAIL} to indicate successful or failed subgoal completion.

Figure 2 (right) illustrates the execution flow. Execution starts at time $t = 0$ by sampling g_0 from π^H . Thereafter, the low-level controller π^L passes the control back to π^H through two actions: (a) a_{PASS} , which adds the subgoal g_k to the subgoal history; or (b) a_{FAIL} , which doesn’t. π^H then computes a new distribution over subgoals to sample the $(k + 1)$ -th subgoal in case of a_{PASS} , or to resample k -th subgoal in case of a_{FAIL} . This process continues until π^H outputs the stop subgoal g_{STOP} or the maximum time horizon is exceeded.

4.1 State Representation

The state representation \hat{s}_t at time t captures the agent’s current understanding of the state of the world, including the locations of objects observed and the agent’s relation to them. The state representation is a tuple $(V_t^S, V_t^O, v_t^S, P_t)$. The semantic map $V_t^S \in [0, 1]^{W \times L \times H \times C}$ is a 3D voxel map

¹We compute P_t and v_t^S using dead-reckoning from RGB observations and actions.

that for every position indicates which of the $c \in [1, C]$ object classes are present in the voxel. The observability map $V_t^O \in \{0, 1\}^{W \times L \times H}$ is a 3D voxel map that indicates whether the corresponding position has been observed. The inventory vector $v_t^S \in \{0, 1\}^C$ indicates which of the C object classes the agent is currently holding. The agent pose $P_t = (x, y, \omega_p, \omega_y)$ is specified by the 2D position (x, y) , pitch angle ω_p , and yaw angle ω_y .

We also compute 2D *state affordance features* $\text{AFFORD}(\hat{s}_t) \in [0, 1]^{7 \times W \times L}$ in a top-down view that represent each position with one or more of seven affordance classes {pickable, receptacle, toggleable, openable, ground, obstacle, observed}. Each $[\text{AFFORD}(\hat{s}_t)]_{(\tau, x, y)} = 1.0$ if at least one of the voxels at position (x, y) has affordance class τ , otherwise it is zero.²

4.2 Observation Model

The observation model $F(\hat{s}_{t-1}, o_t, g_k)$ updates the state representation with new observations. It considers the current subgoal g_k to actively acquire information relevant to g_k . The computation of F consists of three steps: perception, projection, accumulation.

Perception Step We predict semantic segmentation I_t^S and depth map I_t^D from the RGB observation I_t . We use neural networks pre-trained in the ALFRED environment. The semantic segmentation $[I_t^S]_{(u, v)}$ is a distribution over C object classes at pixel (u, v) . The depth map $[I_t^D]_{(u, v)}$ is a binned distribution over B bins.³ We also heuristically compute a binary mask M_t^D that indicates which pixels have confident depth readings. We allow more confidence slack in pixels that correspond to the current subgoal argument \arg_k^C according to I_t^S . Appendix A.1 provides further details. The perception step models are designed to be trained with the limited data available in ALFRED, and can be replaced with more general models given more perception data [40, 41].

Projection Step We use a pinhole camera model to convert depth I_t^D and segmentation I_t^S to a point cloud that represents each image pixel (u, v) with a 3D position $(x, y, z) \in \mathbb{R}^{W \times L \times H}$ and a semantic distribution $[I_t^S]_{(u, v)}$. We use $\arg \max_B(I_t^D)$ to compute the 3D positions, and discard points at pixels (u, v) when the binary mask value is $[M_t^D]_{(u, v)} = 0$. We construct a discrete semantic voxel map $\hat{V}_t^S \in [0, 1]^{W \times L \times H \times C}$, where W , L , and H are the width, height, and length. The value at each voxel $[\hat{V}_t^S]_{(x, y, z)}$ is the element-wise maximum of the segmentation distributions across all points within the voxel. We additionally compute a binary observability map $\hat{V}_t^O \in \{0, 1\}^{W \times L \times H}$ that indicates the voxels observed at time t . A voxel is observed if it contains any points, or if a ray cast from the camera through the voxel centroid has expected depth greater than the distance from the camera to the centroid. Free-space voxels seen through are observed.

Accumulation Step We integrate \hat{V}_t^S and \hat{V}_t^O into a persistent state representation:

$$V_t^S = \hat{V}_t^S \times \hat{V}_{t-1}^S + V_{t-1}^S \times (1 - \hat{V}_t^O) \quad V_t^O = \max(V_{t-1}^O, \hat{V}_t^O) \quad (1)$$

This operation updates each voxel with the most recent semantic distribution, while retaining the values of all voxels not visible at time t . The output of the observation model is the spatial state representation $\hat{s}_t = (V_t^S, V_t^O, v_t^S, P_t)$. The inventory v_t^S and pose P_t are taken directly from o_t .

4.3 High-level Controller (π^H)

At timestep t , when invoked for the k -th time, the input to π^H is the instruction L , the sequence of past subgoals $\langle g_i \rangle_{i < k}$, and the current state representation \hat{s}_t . The output is the next subgoal $g_k = (\text{type}_k, \arg_k^C, \arg_k^M)$. The controller model encodes the three inputs and predicts the subgoal via sampling. Figure 3 illustrates the high-level controller architecture.

Input Encoding We encode the text L using a pre-trained BERT [42] model.⁴ We use the CLS token embedding as the task embedding ϕ^L . We encode the state representation \hat{s}_t to account for classes of all observed objects, and the class of the object that the agent is holding:

²We assume a known mapping between object semantic classes and affordance classes.

³We use B uniformly spaced depth bins $\{0, \Delta_D, 2\Delta_D, \dots, (B-1)\Delta_D\}$, where Δ_D is a depth resolution. We suggest Δ_D should be less than 50% of the voxel size.

⁴During learning, we fine-tune BERT.

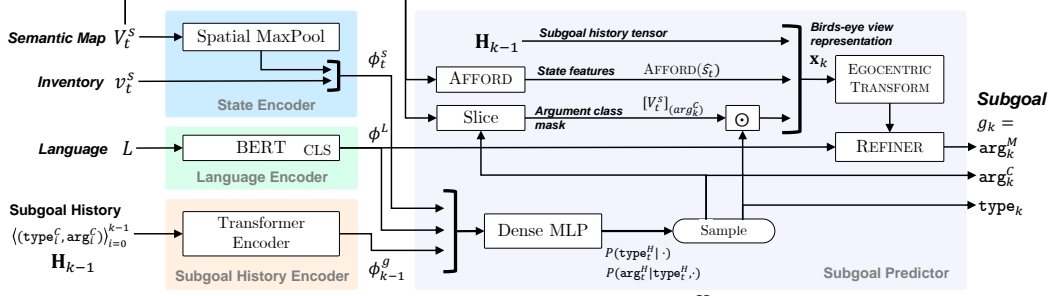


Figure 3: Illustration of the high-level controller π^H (Section 4.3).

$\phi^s(\hat{s}_t) = [v_t^S; \max_{(x,y,z)}(V_t^S)]$, where $\max_{(x,y,z)}$ is a max-pooling operation over spatial dimensions and $[\cdot; \cdot]$ denotes concatenation. We compute the representations of previous subgoals as $\langle \text{REPR}(g_i) \rangle_{i=0}^{k-1}$, where $\text{REPR}(g_i)$ is the sum of a sinusoidal positional encoding [43] of index i and learned embeddings for type_i and arg_i^C . We process this sequence with a two-layer Transformer autoregressive encoder [43] to compute $\langle \phi_i^g \rangle_{i=0}^{k-1}$. We take ϕ_{k-1}^g as the subgoal history embedding vector. We additionally encode the argument mask information arg_i^M from the subgoal history in an integer-valued subgoal history tensor $\mathbf{H}_{k-1} \in \mathbb{N}^{K \times W \times L}$ where $[\mathbf{H}_{k-1}]_{(\tau,x,y)}$ is the number of times an interaction action type τ was performed at 2D position (x, y) in the birds-eye view:

$$[\mathbf{H}_{k-1}]_{(\tau,x,y)} = \sum_{\substack{i=0 \dots k-1 \\ \text{arg}_i^C = \tau}} \max_z ([\text{arg}_i^M]_{(x,y,z)}) . \quad (2)$$

Subgoal Prediction We concatenate the three representations $\mathbf{h}_{(t,k)} = [\phi^L; \phi_t^s; \phi_{k-1}^g]$. We use a densely connected multi-layer perceptron [44] to predict two distributions $P(\text{type}_k | \mathbf{h}_{(t,k)})$ and $P(\text{arg}_k^C | \text{type}_k, \mathbf{h}_{(t,k)})$, from which we sample a subgoal type type_k and argument class arg_k^C .

The remaining component of the subgoal is the action argument mask arg_k^M . Let $[V_t^S]_{(\text{arg}_k^C)}$ be a voxel map that only retains the object information for objects of class arg_k^C in the semantic map V_t^S . We refine it to identify a single object instance. We compute a birds-eye view representation:

$$\mathbf{x}_t = [\text{AFFORD}(\hat{s}_t); \mathbf{H}_{k-1}; \max_z ([V_t^S]_{(\text{arg}_k^C)}) \odot \mathbb{1}_{\text{type}_k}] \quad (3)$$

where $\text{AFFORD}(\hat{s}_t)$ is a birds-eye view state affordance feature map (Section 4.1) and $\mathbb{1}_{\text{type}_k}$ is a one-hot encoding of type_k .⁵ Finally, we compute the 3D argument mask $\text{arg}_k^M \in [0, 1]^{W \times L \times H}$:

$$\text{arg}_k^M = \text{REFINER}(\text{EGOTRANSFORM}(\mathbf{x}_t, P_t), \phi^L) , \quad (4)$$

where $\text{EGOTRANSFORM}(\mathbf{x}, P_t)$ transforms the map \mathbf{x} to the agent egocentric pose P_t , REFINER is a neural network based on the LingUNet architecture [24], and ϕ^L is the language embedding. The refined arg_k^M is a $[0, 1]$ -valued 3D mask that identifies the instance of the interaction argument object. If the object is believed to be unobserved, then arg_k^M contains all zeroes. The controller output is the subgoal $g_k = (\text{type}_k, \text{arg}_k^C, \text{arg}_k^M)$.

4.4 Low-level Controller (π^L)

The low-level controller π^L is conditioned on the most recent subgoal $g_k = (\text{type}_k, \text{arg}_k^C, \text{arg}_k^M)$. At time t , it maps the state representation \hat{s}_t to an action a_t . It combines engineered and learned components. Appendix A.3 provides the implementation details. The controller π^L invokes a set of procedures across multiple time steps t . The procedures are `NavigateTo`, `SampleExplorationPosition`, `SampleInteractionPose`, and `InteractMask`. Their invocation follows a pre-specified execution flow graph across multiple timesteps. First, we perform a 360° rotation to observe the nearby environment. If no objects of type arg_k^C are observed, we explore the environment by sampling a position $(x, y) = \text{SampleExplorationPosition}(\hat{s}_t)$, navigating there using the procedure `NavigateTo`(x, y, \hat{s}_t), and performing a 360° rotation. We repeat exploration until a voxel in V_t^S contains the class arg_k^C with $>50\%$ probability. To interact

⁵ \odot denotes multiplication of a $X \times Y$ tensor with a K -dimensional vector to obtain a $K \times X \times Y$ tensor. $[\cdot; \cdot; \cdot]$ denotes channel-wise concatenation.

with an object, we sample an interaction pose $(x, y, \omega_y, \omega_p) = \text{SampleInteractionPose}(\hat{s}_t, g_k)$, invoke $\text{NavigateTo}(x, y, \hat{s}_t)$ to reach the position (x,y), and then rotate according to yaw and pitch angles (ω_y, ω_p) . Finally, we generate the egocentric interaction action mask $\text{mask}_t = \text{InteractMask}(\hat{s}_t, \text{arg}_k^M)$, and output the interaction action $(\text{type}_k, \text{mask}_t)$.

All procedures use the spatial representation \hat{s}_t . NavigateTo navigates to a goal position using a value iteration network (VIN) [45] that reasons over obstacle and observability maps from \hat{s}_t . $\text{SampleExplorationPosition}$ samples positions on the boundary of observed space in \hat{s}_t . $\text{SampleInteractionPose}$ uses a learned neural network NAVMODEL to predict a distribution of poses from which the interaction g_k will likely succeed. InteractMask uses the segmentation image I_t^S and the 3D argument mask arg_t^M to compute the first-person mask of the target object.

5 Learning

The policy contains four learned models: the segmentation and depth networks, the high-level controller π^H , and the navigation model NAVMODEL used by the low-level controller. We train all networks using supervised learning. We assume access to a training dataset $\mathcal{D} = \{(L^{(j)}, \Xi^{(j)})\}_{j=1}^{N_D}$ of natural language instructions $L^{(j)}$ paired with demonstration execution $\Xi^{(j)}$ in a set of seen environments. Each execution $\Xi^{(j)}$ is a sequence of states and actions $\langle s_0^{(j)}, a_0^{(j)}, \dots, s_T^{(j)}, a_T^{(j)} \rangle$. We denote N_P the total number of states in \mathcal{D} , and N_G the total number of subgoals.

We process \mathcal{D} into three datasets. The perception dataset $\mathcal{D}^P = \{([I]^{(i)}, [I^D]^{(i)}, [I^S]^{(i)})\}_{i=1}^{N_P}$ includes RGB images $[I]^{(i)}$ with ground truth depth $[I^D]^{(i)}$ and segmentation $[I^S]^{(i)}$. The subgoal dataset $\mathcal{D}^g = \{(L^{(i)}, \hat{s}_t^{(i)}, \langle g_j^{(i)} \rangle_{j=0}^k)\}_{i=1}^{N_G}$ contains natural language instructions $L^{(i)}$, state representations $\hat{s}_t^{(i)}$ at the start of k -th subgoal execution, and sequences of the first k subgoals $\langle g_j^{(i)} \rangle_{j=0}^k$. The navigation dataset $\mathcal{D}^N = \{(\hat{s}^{(i)}, g^{(i)}, P^{(i)})\}_{i=1}^{N_P}$ consists of state representations $\hat{s}^{(i)}$, subgoals $g^{(i)}$, and agent poses $P^{(i)}$ at the time of taking the interaction action corresponding to subgoal $g^{(i)}$. The state representations $\hat{s}^{(\cdot)}$ in datasets \mathcal{D}^g and \mathcal{D}^N are constructed using the observation model (Section 4.2), but using ground-truth depth and segmentation images.

We train the perception models on \mathcal{D}^P and the π^H on \mathcal{D}^g to predict the k -th subgoal by optimizing cross-entropy losses. We use \mathcal{D}^N to train the navigation model NAVMODEL by optimizing a cross-entropy loss for positions and yaw angles, and an L2 loss for the pitch angle.

6 Experimental Setup

Environment, Data, and Evaluation We evaluate our approach on the ALFRED [10] benchmark of indoor scenes. The scenes are split to 108 training scenes, 88/4 validation seen/unseen scenes, and 107/8 test seen/unseen scenes. There are 21,023 training tasks, 820/821 validation seen/unseen tasks, and 1533/1529 test seen/unseen tasks. Each task is specified with a high-level natural language instruction. The goal of the agent is to map raw RGB observations to actions to complete the task. ALFRED also provides detailed low-level step-by-step instructions, which simplify the reasoning process. We do not use these instructions for training or evaluation. We collect a training dataset of language-demonstration pairs for learning (Section 5). To extract subgoal sequences, we label each interaction action $a_t = (\text{type}_t, \text{mask}_t)$ and any preceding navigation actions with a single subgoal of $\text{type} = \text{type}_t$. We compute the subgoal argument class arg^C and 3D mask arg^M labels from the first-person mask mask_t , and ground truth segmentation and depth images. Completing a task requires satisfying several goal conditions. Following the common evaluation [46, 47], we report two metrics. *Success rate* (SR) is the fraction of tasks for which all goal conditions were satisfied. *Goal condition rate* (GC) is the fraction of goal-conditions satisfied across all tasks.

Systems We compare our approach, the Hierarchical Language-conditioned Spatial Model (HLSM) to others on the ALFRED leaderboard that only use the high-level instructions. At the time of writing, the only such published approach is HiTUT [37], a hierarchical approach that directly reasons over first-person images instead of computing a spatial representation. We also compare to approaches that use the sequential step-by-step instructions, which puts our method at a disadvantage.

Additionally, we perform ablations and study sensory oracles. To study the observation model, we compare to using sensory oracles for ground truth depth, ground truth segmentation, and both. We

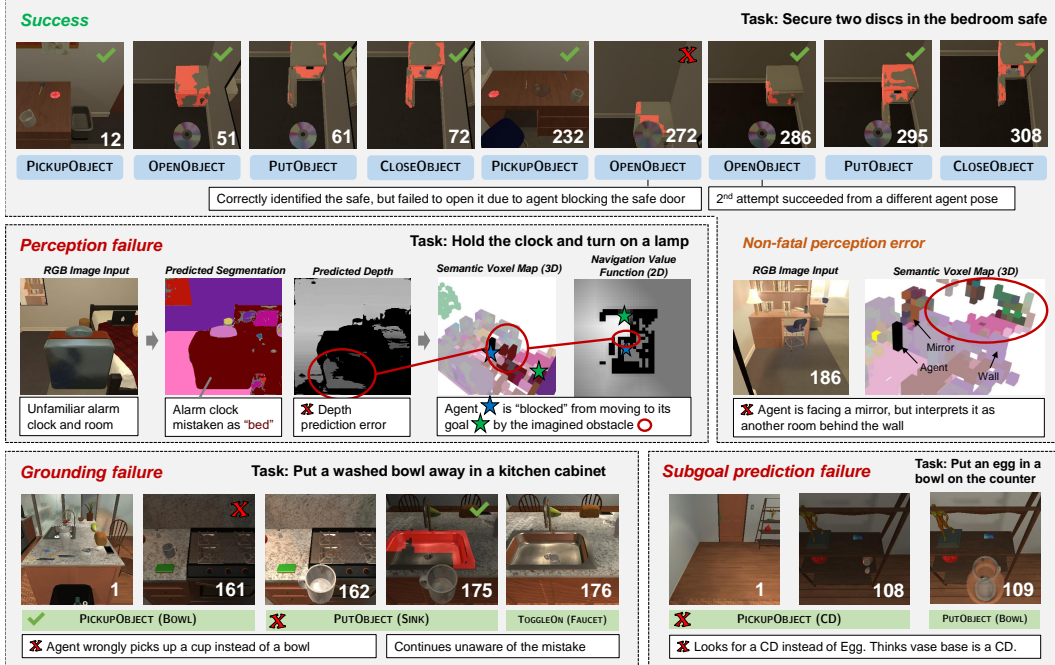


Figure 4: Qualitative results showcasing successes and failures of our approach. **Top row:** snapshots of every interaction action taken during a successful task. Action argument masks are overlaid in red over the RGB images. The white numbers are timesteps. **Middle-right:** illustration of a non-fatal perception error. **Middle-left:** illustration of a fatal perception error. The agent incorrectly interprets the reflection on the alarm clock as an obstacle. The obstacle is represented in the semantic map, causing the agent (blue star) to believe that the path to the goal (green star) is blocked off. This is reflected in the navigation value function computed by the value iteration network (VIN) [45], where black cells are obstacles with value -1 . White cell is the goal with value 1 . **Bottom-left:** grounding failure. The agent wrongly picks up the cup instead of a bowl. Predicted subgoals are shown in green. **Bottom-right:** high-level controller and perception failure. π^H predicts the wrong subgoal argument class (CD instead of EGG). The segmentation model then mistakes the vase for a CD.

report high-level controller ablations that remove the subgoal encoder, language encoder, and state representation encoder as used for predicting subgoal type type_k and argument class arg_k^C , while still using the state representation \hat{s}_t to predict the subgoal argument mask arg_k^M . We also study a low-level controller ablation that removes the exploration procedure.

7 Results

Table 1 shows test and validation results. Our approach achieves state-of-the-art performance across both seen and unseen environments in the setting with only high-level instructions. We achieve 6.06% absolute (59.2% relative) improvement in SR on the test unseen split, and 6.7% absolute (36.4% relative) improvement in SR on the test seen split compared to HiTUT G-only.

Our approach performs competitively even when compared to approaches that also use the low-level step-by-step instructions. We achieve 0.86% absolute (5.6% relative) improvement in SR on the test unseen split compared to ABP [11].⁶ On the test seen split, our approach performs reasonably well, however ABP [11], E.T. [12], and LWIT [13] perform better, reflecting stronger scene overfitting.

Tables 2 and 3 show development results. Using ground truth depth (+ gt depth) provides 3.2%/1% absolute improvement in seen/unseen environments. Using ground truth segmentation (+ gt seg) provides 16.3%/19.3% absolute improvement. Using both ground truth depth and segmentation (+ gt depth, gt seg) provides 19.1%/30.2% absolute improvement, and narrows the seen/unseen gap from 13.2% to 2.1%. This shows that perception is the biggest generalization bottleneck.

We report high-level controller π^H input encoder ablations. The poor performance without the language encoder reflects task difficulty. Sampling and executing random subgoals without language input seldom solves the task. Zeroing the input to the subgoal history encoder (but keeping position encodings) reduces performance by only 1.7%/1.8%, showing that knowing the index of the

⁶The details and validation results of the ABP and LAV models were not published at the time of writing.

Method	Test				Validation			
	Seen		Unseen		Seen		Unseen	
	SR	GC	SR	GC	SR	GC	SR	GC
Low-level Sequential Instructions + High-level Goal Instruction								
SEQ2SEQ [10]	3.98	9.42	0.39	7.03	3.70	10.00	0.00	6.90
MOCA [36]	22.05	28.29	5.30	14.28	19.15	28.5	3.78	13.4
E.T. [12]	28.77	36.47	5.04	15.01	33.78	42.48	3.17	13.12
E.T. + synth. data [12]	38.42	45.44	8.57	18.6	46.59	52.82	7.32	20.87
LWIT [48]	30.92	45.44	9.42	20.91	33.70	43.10	9.70	23.10
HiTUT[37]	21.27	29.97	13.87	20.31	25.24	34.85	12.44	23.71
ABP [11] ⁶	44.55	51.13	15.43	24.76	-	-	-	-
High-level Goal Instruction Only								
HiTUT G-only[37]	18.41	25.27	10.23	20.27	13.63	21.11	11.12	17.89
LAV [49] ⁶	13.35	23.21	6.38	17.27	-	-	-	-
HLSTM (Ours)	25.11	35.79	16.29	27.24	25.00	36.37	11.80	24.70

Table 1: Test results. Test seen/unseen and validation seen/unseen splits. Top section approaches use sequential step-by-step instructions. The bottom section uses only high-level instructions.

Method	Validation				Task Type	Validation			
	Seen		Unseen			Seen		Unseen	
	SR	GC	SR	GC		SR	GC	SR	GC
HLSTM	25.0	36.4	11.8	24.7	Overall	25.0	36.4	11.8	24.7
+ gt depth	28.2	36.7	12.8	26.2	Examine	37.2	55.9	22.5	45.7
+ gt depth, gt seg.	44.1	54.5	42.0	53.2	Pick & Place	42.3	42.3	28.0	28.0
+ gt seg.	41.3	51.6	31.1	43.2	Stack & Place	8.7	23.1	1.8	7.0
w/o language enc.	0.6	8.3	0.2	7.6	Clean & Place	25.0	43.8	10.6	25.3
w/o subg. hist. enc.	23.3	31.8	10.0	22.8	Cool & Place	11.9	29.9	3.7	22.9
w/o state repr enc.	23.8	34.3	12.9	25.7	Heat & Place	12.1	29.1	0.0	14.1
w/o exploration	24.9	35.9	11.3	23.7	Pick 2 & Place	35.5	50.8	12.3	29.2

Table 2: Development results on validation split. Performance of our full approach, with perception oracles, a perception ablation, π^H ablations, and π^L ablations

Table 3: Performance breakdown per task type on the validation split.

current subgoal in addition to the state representation is often sufficient. Not using the state representation for predicting subgoal type and argument class reduces SR by 1.7% in seen scenes, but increases SR by 1.1% in unseen scenes, achieving state-of-the-art validation-unseen SR of 12.9% in the sequential+high-level instruction setting. This shows that predicting the sequence of subgoal types and argument classes (i.e., what to do) is at times possible without spatial reasoning, while grounding the subgoal (i.e., where to do it) requires spatial information. Removing random exploration from π^L reduces SR by 0.1%/0.5% on seen/unseen scenes, showing it is not very effective.

Figure 4 illustrates the model behavior, showing both successes and common failures. The main failures in valid unseen scenes are due to (1) perception errors that result in missing or extraneous obstacles or picking up wrong objects; (2) insufficiency of random exploration (e.g., not searching inside cabinets); (3) navigation model errors (e.g., blocking objects from opening); (4) subgoal prediction errors (e.g., picking up wrong objects); and (5) lack of state-aware multi-step planning and backtracking. More qualitative results are available in Appendix A.7.

8 Discussion

We showed that a persistent spatial semantic representation enables a hierarchical model to achieve state-of-the-art performance on a challenging instruction-following mobile manipulation task. As we did not place significant focus on the low-level controller procedures, improving them to better utilize our spatial representation is an important direction for future research. For example, learning exploration or navigation models instead of using hand-coded primitives could improve robustness. In terms of perception, better segmentation and depth prediction in unseen environments is an area of possible improvement. Finally, incorporating reinforcement learning to train the high-level controller, low-level controller, and observation model jointly could improve robustness of the approach.

References

- [1] S. Tellex, T. Kollar, S. Dickerson, M. R. Walter, A. Gopal Banerjee, S. Teller, and N. Roy. "Approaching the Symbol Grounding Problem with Probabilistic Graphical Models. *AI Magazine*, 2011.
- [2] C. Matuszek, E. Herbst, L. Zettlemoyer, and D. Fox. Learning to parse natural language commands to a robot control system. In *ISER*, 2012.
- [3] D. K. Misra, J. Sung, K. Lee, and A. Saxena. Tell me dave: Context-sensitive grounding of natural language to mobile manipulation instructions. In *RSS*, 2014.
- [4] J. Thomason, S. Zhang, R. J. Mooney, and P. Stone. Learning to interpret natural language commands through human-robot dialog. In *IJCAI*, 2015.
- [5] D. Misra, J. Langford, and Y. Artzi. Mapping instructions and visual observations to actions with reinforcement learning. In *EMNLP*, 2017.
- [6] D. Nyga, S. Roy, R. Paul, D. Park, M. Pomarlan, M. Beetz, and N. Roy. Grounding robot plans from natural language instructions with incomplete world knowledge. In *CoRL*, 2018.
- [7] V. Blukis, N. Brukhim, A. Bennet, R. Knepper, and Y. Artzi. Following high-level navigation instructions on a simulated quadcopter with imitation learning. In *RSS*, 2018.
- [8] V. Blukis, D. Misra, R. A. Knepper, and Y. Artzi. Mapping navigation instructions to continuous control actions with position-visitation prediction. In *CoRL*, 2018.
- [9] V. Blukis, Y. Terme, E. Niklasson, R. A. Knepper, and Y. Artzi. Learning to map natural language instructions to physical quadcopter control using simulated flight. In *CoRL*, 2019.
- [10] M. Shridhar, J. Thomason, D. Gordon, Y. Bisk, W. Han, R. Mottaghi, L. Zettlemoyer, and D. Fox. Alfred: A benchmark for interpreting grounded instructions for everyday tasks. In *CVPR*, 2020.
- [11] B. Kim, S. Bhambri, K. P. Singh, R. Mottaghi, and J. Choi. Abp, alfred leaderboard, may 10th 2021. <https://leaderboard.allenai.org/alfred/submission/c2t70j37q4q5ci4so89g>. Accessed: June 16th, 2021.
- [12] A. Pashevich, C. Schmid, and C. Sun. Episodic Transformer for Vision-and-Language Navigation, 2021.
- [13] Anonymous. Lwit, alfred leaderboard, may 10th 2021. <https://leaderboard.allenai.org/alfred/submission/bvppcin94ro4j7j0jq1g>. Accessed: May 25th, 2021.
- [14] I. Kostavelis and A. Gasteratos. Semantic mapping for mobile robotics tasks: A survey. *Robotics and Autonomous Systems*, 2015.
- [15] T. Kollar, S. Tellex, D. Roy, and N. Roy. Toward understanding natural language directions. In *HRI*, 2010.
- [16] C. Matuszek, N. FitzGerald, L. Zettlemoyer, L. Bo, and D. Fox. A Joint Model of Language and Perception for Grounded Attribute Learning. In *ICML*, 2012.
- [17] R. A. Knepper, S. Tellex, A. Li, N. Roy, and D. Rus. Recovering from Failure by Asking for Help. *Autonomous Robots*, 2015.
- [18] T. Brick and M. Scheutz. Incremental natural language processing for hri. In *HRI*, 2007.
- [19] K. M. Hermann, F. Hill, S. Green, F. Wang, R. Faulkner, H. Soyer, D. Szepesvari, W. Czarnecki, M. Jaderberg, D. Teplyashin, et al. Grounded language learning in a simulated 3d world. *arXiv preprint arXiv:1706.06551*, 2017.
- [20] D. S. Chaplot, K. M. Sathyendra, R. K. Pasumarthi, D. Rajagopal, and R. Salakhutdinov. Gated-attention architectures for task-oriented language grounding. *AAAI*, 2018.

- [21] C. Paxton, Y. Bisk, J. Thomason, A. Byravan, and D. Fox. Prospection: Interpretable plans from language by predicting the future. In *ICRA*, 2019.
- [22] P. Anderson, Q. Wu, D. Teney, J. Bruce, M. Johnson, N. Sünderhauf, I. Reid, S. Gould, and A. van den Hengel. Vision-and-language navigation: Interpreting visually-grounded navigation instructions in real environments. In *CVPR*, 2018.
- [23] D. Fried, R. Hu, V. Cirik, A. Rohrbach, J. Andreas, L.-P. Morency, T. Berg-Kirkpatrick, K. Saenko, D. Klein, and T. Darrell. Speaker-follower models for vision-and-language navigation. In *NeurIPS*, 2018.
- [24] D. Misra, A. Bennett, V. Blukis, E. Niklasson, M. Shatkin, and Y. Artzi. Mapping instructions to actions in 3D environments with visual goal prediction. In *EMNLP*, 2018.
- [25] C.-Y. Ma, J. Lu, Z. Wu, G. AlRegib, Z. Kira, R. Socher, and C. Xiong. Self-monitoring navigation agent via auxiliary progress estimation. In *ICLR*, 2019.
- [26] H. Tan, L. Yu, and M. Bansal. Learning to navigate unseen environments: Back translation with environmental dropout. In *NAACL-HLT*, 2019.
- [27] H. Chen, A. Suhr, D. Misra, and Y. Artzi. Touchdown: Natural language navigation and spatial reasoning in visual street environments. In *CVPR*, 2019.
- [28] D. K. Misra, K. Tao, P. Liang, and A. Saxena. Environment-driven lexicon induction for high-level instructions. In *ACL*, 2015.
- [29] M. MacMahon, B. Stankiewicz, and B. Kuipers. Walk the talk: Connecting language, knowledge, and action in route instructions. In *AAAI*, 2006.
- [30] S. R. K. Branavan, L. S. Zettlemoyer, and R. Barzilay. Reading between the lines: Learning to map high-level instructions to commands. In *ACL*, 2010.
- [31] F. Duvallet, T. Kollar, and A. Stentz. Imitation learning for natural language direction following through unknown environments. In *ICRA*, 2013.
- [32] M. R. Walter, S. Hemachandra, B. Homberg, S. Tellex, and S. Teller. Learning Semantic Maps from Natural Language Descriptions. In *RSS*, 2013.
- [33] Y. Artzi and L. Zettlemoyer. Weakly supervised learning of semantic parsers for mapping instructions to actions. *TACL*, 2013.
- [34] S. Hemachandra, F. Duvallet, T. M. Howard, N. Roy, A. Stentz, and M. R. Walter. Learning models for following natural language directions in unknown environments. In *ICRA*, 2015.
- [35] E. C. Williams, N. Gopalan, M. Rhee, and S. Tellex. Learning to parse natural language to grounded reward functions with weak supervision. In *ICRA*, 2018.
- [36] K. P. Singh, S. Bhambri, B. Kim, R. Mottaghi, and J. Choi. Moca: A modular object-centric approach for interactive instruction following. *arXiv preprint arXiv:2012.03208*, 2020.
- [37] Y. Zhang and J. Chai. Hierarchical task learning from language instructions with unified transformers and self-monitoring. *ACL Findings*, 2021.
- [38] D. Gordon, A. Kembhavi, M. Rastegari, J. Redmon, D. Fox, and A. Farhadi. Iqa: Visual question answering in interactive environments. In *CVPR*, 2018.
- [39] P. Anderson, A. Shrivastava, D. Parikh, D. Batra, and S. Lee. Chasing ghosts: Instruction following as bayesian state tracking. In *NeurIPS*, 2019.
- [40] J. McCormac, A. Handa, S. Leutenegger, and A. J. Davison. Scenenet rgb-d: Can 5m synthetic images beat generic imagenet pre-training on indoor segmentation? In *ICCV*, 2017.
- [41] Y. Wu, A. Kirillov, F. Massa, W.-Y. Lo, and R. Girshick. Detectron2. <https://github.com/facebookresearch/detectron2>, 2019.

- [42] J. Devlin, M.-W. Chang, K. Lee, and K. Toutanova. Bert: Pre-training of deep bidirectional transformers for language understanding. In *NAACL*, 2019.
- [43] A. Vaswani, N. Shazeer, N. Parmar, J. Uszkoreit, L. Jones, A. N. Gomez, Ł. Kaiser, and I. Polosukhin. Attention is all you need. In *NeurIPS*, 2017.
- [44] G. Huang, Z. Liu, L. van der Maaten, and K. Q. Weinberger. Densely connected convolutional networks. In *CVPR*, 2017.
- [45] A. Tamar, Y. Wu, G. Thomas, S. Levine, and P. Abbeel. Value iteration networks. In *NeurIPS*, 2016.
- [46] M. Shridhar and D. Hsu. Interactive visual grounding of referring expressions for human-robot interaction. In *RSS*, 2018.
- [47] M. Shridhar, J. Thomason, D. Gordon, Y. Bisk, W. Han, R. Mottaghi, L. Zettlemoyer, and D. Fox. Alfred leaderboard. <https://leaderboard.allenai.org/alfred/>. Accessed: June 16th, 2021.
- [48] V.-Q. Nguyen, M. Suganuma, and T. Okatani. Look wide and interpret twice: Improving performance on interactive instruction-following tasks. In *IJCAI*, 2021.
- [49] K. Nottingham, L. Liang, D. Shin, C. C. Fowlkes, R. Fox, and S. Singh. Lav, alfred leaderboard, may 10th 2021. <https://leaderboard.allenai.org/alfred/submission/c2cm7eranqs9puf9uvjg>. Accessed: May 25th, 2021.
- [50] O. Ronneberger, P. Fischer, and T. Brox. U-net: Convolutional networks for biomedical image segmentation. In *MICCAI*, 2015.

A Appendix

A.1 Observation Model Details

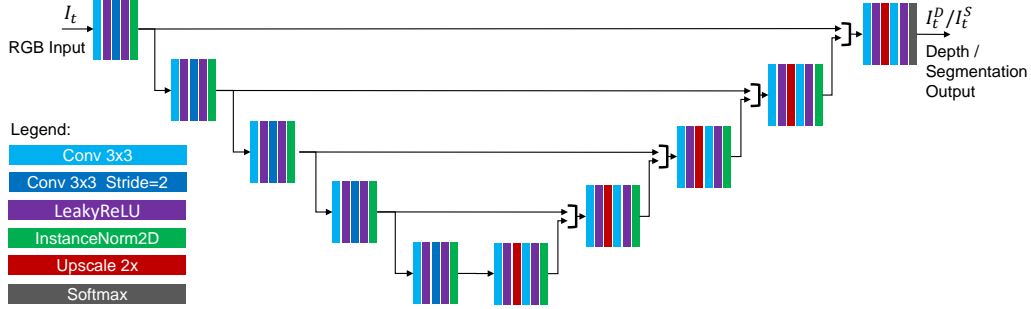


Figure 5: Illustration of the U-Net architecture used in the depth and segmentation networks.

At time t , during the perception step, we predict first-person semantic segmentation I_t^S and depth I_t^D from the observation $o_t = (I_t, P_t, v_t^S, L)$, from the RGB image I_t with neural network models pre-trained in the ALFRED environment. Each pixel $[I_t^S]_{(u,v)}$ at coordinates (u, v) is a distribution over C object classes. Likewise, $[I_t^D]_{(u,v)}$ is a distribution over B uniformly spaced depth bins $\{0, \Delta_D, 2\Delta_D, \dots, (B-1)\Delta_D\}$, where Δ_D is a depth resolution. In early experiments, we observed that Δ_D should be less than 50% of the voxel size. We use $\Delta_D = 0.1m$, $B = 50$, and voxel size of $0.25m$. We also heuristically compute a binary mask M_t^D that indicates which pixels have confident depth readings. We allow more confidence slack in pixels that correspond to the current subgoal argument \arg_t^C according to I_t^S . The mask M_t^D is used in the projection step to discard points (x, y, z) that correspond to pixels (u, v) for which $[M^D]_{(u,v)} = 0$. The mask computation is:

$$M_t^D = (W_{90}[I_t^D] < c_1 \mathbb{E}[I_t^D]) \vee ((W_{90}[I_t^D] < c_2 \mathbb{E}[I_t^D]) \wedge ([I_t^S]_{\arg_t^C} > 0.5)) \quad , \quad (5)$$

where $W_{90}[I_t^D]$ is the width of the 90% confidence interval at each pixel, $\mathbb{E}[I_t^D]$ is the expected depth at each pixel, and $[I_t^S]_{\arg_t^C}$ is a 0-1 valued segmentation mask of the class of the current subgoal argument. We set the hyperparameters $c_1 = 0.3$ and $c_2 = 1.0$ to allow higher depth uncertainty for points corresponding to the subgoal argument.

If the agent is currently holding an object (i.e. $\sum_i [[v_t^S]_{(i)}] > 0$), we also discard points closer than $0.7m$ to the camera to make sure that the object in the agent inventory does not get added to the voxel map.

We use custom models based on the U-Net architecture [50] for depth and segmentation networks. The architecture is illustrated in Figure 5. It consists of a cascade of five downscale blocks followed by five upscale blocks with skip-connections. Each block includes two convolutions, two leakyReLU activations, and an instance normalization layer. The upscale blocks contain a 2x spatial upscaling operation. We found that training a separate network for depth and segmentation worked better than sharing one network for both tasks.

A.2 High-Level Controller Details

Subgoals are predicted periodically. Let $g_k = (\text{type}_k, \arg_k^C, \arg_k^M)$ be the k -th subgoal predicted at time t . Predicting the subgoal type type_k and the argument class \arg_k^C is described in the main paper (Section 4.3). This section provides further details of REFINER, the model we use to generate \arg_k^M . The mask refiner REFINER has four inputs:⁷ (a) a spatial feature map $\mathbf{x}_t^{ego} \in [0, 1]^{N \times W \times L}$ oriented in the agent egocentric reference frame; (b) $[V_t^S]_{(\arg_k^C)} \in [0, 1]^{W \times L \times H}$, a 3D mask indicating all voxels that contain objects of class \arg_k^C in the voxel map V_t^S ; (c) the agent’s pose P_t ; and (d) a vector representation of the instruction ϕ^L . It outputs a 3D mask $\arg_k^M \in$

⁷Errata: Equation 4 in the main paper is missing $[V_t^S]_{(\arg_k^C)}$ and P_t arguments to the REFINER.

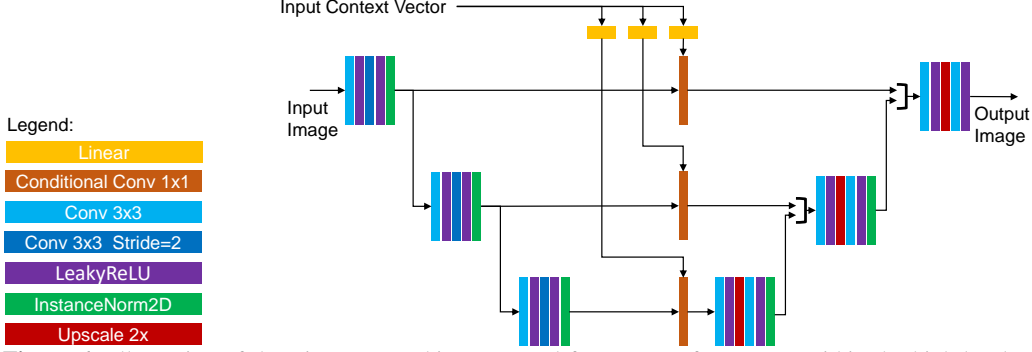


Figure 6: Illustration of the LingUNet architecture used for as part of REFINER within the high-level controller π^H , and as part of the navigation model NAVMODEL within the low-level controller. The conditional convolutions parameters are computed during the network forward pass.

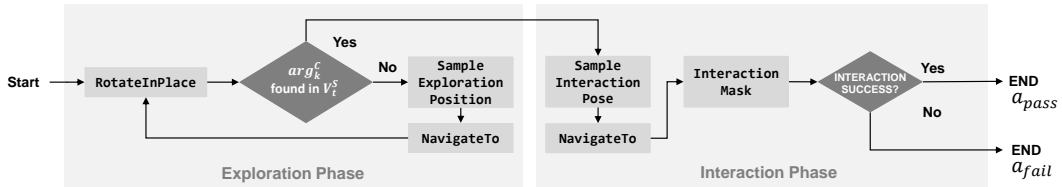


Figure 7: Illustration of the low-level controller execution flow, showing the order in which procedures are used to complete a subgoal g_k .

$[0, 1]^{W \times L \times H}$ that identifies the subgoal argument object. Formally, the computation is:⁸

$$\begin{aligned} \text{REFINER}(\mathbf{x}_t^{ego}, [V_t^S]_{(\arg_k^C)}, P_t, \phi^L) = \\ \text{ALLOTRANSFORM}(\text{LINGUNET}_m(\mathbf{x}_t^{ego}, \phi^L), P_t) \otimes [V_t^S]_{(\arg_k^C)}, \end{aligned} \quad (6)$$

where ALLOTRANSFORM transforms a spatial 2D map from an egocentric to the global reference frame, and LINGUNET_m is a language-conditioned image-to-image encoder-decoder [24]. The architecture of LINGUNET_m is illustrated in Figure 6.

A.3 Low-Level Controller Details

We describe the implementation of each of the low-level controller procedures. This implementation is not the focus of this paper, and could be improved or replaced with other algorithms. Some of the procedures cause actions in the AI2Thor environment, others simply process data to pass between procedures.

The procedures are NavigateTo, SampleExplorationPosition, SampleInteractionPose, and InteractMask. The low-level controller receives the subgoal g_k , and follows a pre-specified execution flow across multiple timesteps to complete it. The execution flow (Figure 7) consists of an *exploration* and *interaction* phase. In the exploration phase, we perform a 360° rotation by generating a sequence of three ROTATELEFT actions to observe the environment and add information to the semantic map. If the semantic map indicates that no object of type \arg_k^C , the action argument, is observed, we explore the environment by sampling a position $(x, y) = \text{SampleExplorationPosition}(\hat{s}_t)$, navigating there using $\text{NavigateTo}(x, y, \hat{s}_t)$, and performing another 360° rotation. We repeat this process until a voxel in V_t^S contains the class \arg_k^C with $>50\%$ probability, at which point we move on to the interaction phase. In the interaction phase, we sample an interaction pose $(x, y, \omega_y, \omega_p) = \text{SampleInteractionPose}(\hat{s}_t, g_k)$, invoke $\text{NavigateTo}(x, y, \hat{s}_t)$ to reach the position (x,y), and rotate according to yaw and pitch angles (ω_y, ω_p) . Finally, we generate the egocentric interaction action mask $\text{mask}_t = \text{InteractMask}(\hat{s}_t, \arg_k^M)$, and execute the interaction action $(\text{type}_k, \text{mask}_t)$ in the ALFRED environment. We output a_{PASS} or a_{FAIL} depending if the interaction action has succeeded, and pass control back to the high-level controller to sample the next subgoal.

⁸ \otimes is an operation that multiplies a $W \times L$ matrix by a $W \times L \times H$ tensor to obtain a $W \times L \times H$ tensor

Current Heading	VIN Action	AI2Thor Action
North	WEST	ROTATELEFT
	NORTH	MOVEAHEAD
	EAST or SOUTH	ROTATERIGHT
East	NORTH	ROTATELEFT
	EAST	MOVEAHEAD
	SOUTH or WEST	ROTATERIGHT
South	EAST	ROTATELEFT
	SOUTH	MOVEAHEAD
	WEST or NORTH	ROTATERIGHT
West	SOUTH	ROTATELEFT
	WEST	MOVEAHEAD
	NORTH or EAST	ROTATERIGHT

Table 4: Mapping from VIN actions to AI2Thor actions.

A.3.1 NavigateTo Procedure

At time t , the `NavigateTo` procedure maps a 2D navigation goal position (x, y) and the state representation \hat{s}_t to one of the actions: $\{\text{ROTATELEFT}, \text{ROTATERIGHT}, \text{MOVEAHEAD}, a_{\text{STOP}}\}$. We implement it with a Value Iteration Network [VIN; 45] that solves a 2D grid-MDP to predict navigation actions using fast GPU-accelerated convolution and max-pooling operations. The VIN parameters are pre-defined, and not learned. Other motion planners such as A* could be used as well.

The VIN is defined by a state-space \mathcal{S}^{vin} , action space \mathcal{A}^{vin} , transition function $\mathcal{T}^{vin} : \mathcal{S}^{vin} \times \mathcal{A}^{vin} \rightarrow \mathcal{S}^{vin}$, a reward function $R^{vin} : \mathcal{S}^{vin} \times \mathcal{A}^{vin} \rightarrow \mathbb{R}$, and terminal state set \mathcal{M}^{vin} . At each timestep t , VIN performs value iteration to compute the Q-function $Q^{vin} : \mathcal{S}^{vin} \times \mathcal{A}^{vin} \rightarrow \mathbb{R}$ that estimates the expected sum of future discounted rewards for taking action $a_t^{vin} \in \mathcal{A}^{vin}$ in state $s_t^{vin} \in \mathcal{S}^{vin}$, and thereafter following a greedy policy: $a_i^{vin} = \arg \max_{a^{vin} \in \mathcal{A}^{vin}} Q(s_i^{vin}, a^{vin})$, $i > t$. We implement the state space \mathcal{S}^{vin} as a 2D grid of shape $W^{vin} \times H^{vin}$. Each state s^{vin} is tagged with three 0-1 valued attributes: OBSTACLE, UNOBSERVED, GOAL. At each timestep t , we set the values of state attributes according to the most recent state representation \hat{s}_t and current navigation goal (x, y) . States s^{vin} with occupied voxels in the height range $[0, 1.75m]$ are tagged $\text{OBSTACLE}(s^{vin}) = 1$, otherwise $\text{OBSTACLE}(s^{vin}) = 0$. States with all voxels unobserved are tagged $\text{UNOBSERVED}(s^{vin}) = 1$, otherwise $\text{UNOBSERVED}(s^{vin}) = 0$. The state at the goal position is tagged $\text{GOAL}(s^{vin}) = 1$, for all others $\text{GOAL}(s^{vin}) = 0$. The action space is $\mathcal{A}^{vin} = \{\text{NORTH}, \text{EAST}, \text{SOUTH}, \text{WEST}, \text{STOP}\}$. The transition function encodes epsilon-greedy grid navigation dynamics: (1) the action NORTH moves the agent one state north and likewise for other actions, and (2) with probability $\epsilon = 8\%$ a random transition to a neighboring state occurs. Visiting any terminal state $s^{vin} \in \mathcal{M}^{vin}$ or executing the action STOP terminates the episode. Terminal states are all states tagged with attributes OBSTACLE and GOAL, $\mathcal{M}^{vin} = \{s^{vin} \in \mathcal{S}^{vin} \mid (\text{OBSTACLE}(s^{vin}) > 0.5) \wedge (\text{GOAL}(s^{vin}) > 0.5)\}$.

The reward function assigns different rewards for visiting states with different attributes:

$$R^{vin}(s^{vin}, a^{vin}) = -0.9 \cdot \text{OBSTACLE}(s^{vin}) + 1.0 \cdot \text{GOAL}(s^{vin}) - 0.02 \cdot \text{UNOBSERVED}(s^{vin}) + 0.001 \cdot \mathbb{1}_{a^{vin}=\text{STOP}} \quad (7)$$

OBSTACLE states receive reward -0.9 , GOAL states receive reward 1.0 , and UNOBSERVED states receive reward -0.02 . Taking the STOP action in any state gives reward 0.001 , which has the effect of the agent stopping in unsolvable cases. We use the VIN iteratively for N^{vin} iterations, and predict an action $a^{vin} = \arg \max_{a^{vin} \in \mathcal{A}^{vin}} (Q^{vin}(s_t^{vin}, a^{vin}))$. We map from the VIN action a^{vin} to a single valid AI2Thor navigation action using a deterministic mapping (Table 4).

A.3.2 SampleExplorationPosition

The `SampleExplorationPosition` procedure maps a state representation \hat{s}_t to a discrete 2D position $p^{\text{explore}} = (x, y)$. Let \mathcal{P}_s be the set of 2D positions corresponding to voxel centroids in the voxel map along the horizontal axes, and the ground set \mathcal{P}_g as the set of all unoccupied positions

that have the class FLOOR or RUG in at least one voxel. A position is unoccupied if all voxels in the height range $[0, 1.75m]$ are free of obstacles. We define a frontier set \mathcal{P}_f as the set of all positions \mathcal{P}_g for which at least one immediately neighboring position contains zero observed voxels. If \mathcal{P}_f is non-empty, we sample the position p^{explore} uniformly at random from \mathcal{P}_f . Otherwise, we sample p^{explore} uniformly at random from \mathcal{P}_g .

A.3.3 SampleInteractionPose

The SampleInteractionPose procedure maps the state representation \hat{s}_t and subgoal $g_k = (\text{type}_k, \text{arg}_k^C, \text{arg}_k^M)$ to a pose $P = (x, y, \omega_y, \omega_p)$, where (x, y) is a discrete 2D position, ω_y is the agent yaw angle, and ω_p is the agent camera pitch angle. The pose is predicted such that upon reaching it, the interaction action of type type_k is likely to succeed on the object of class arg_k^C at location identified by the mask arg_k^M .

We use a neural network model NAVMODEL to predict expected pitch $\mathbb{E}(\omega_p|x, y; g_k, \hat{s}_t)$ and a distribution $P(x, y, \omega_y|g_k, \hat{s}_t)$, factored as:

$$P(x, y, \omega_y|g_k, \hat{s}_t) = P(\omega_y|x, y; g_k, \hat{s}_t)P(x, y|g_k, \hat{s}_t) \quad (8)$$

The network NAVMODEL is based on the LingUNet architecture (Figure 6):

$$\text{NAVMODEL}(\hat{s}_t, g_k) = \text{LINGUNET}(\text{AFFORD}(\hat{s}_t), \text{LINEAR}([\text{LUT}_T(\text{type}_k); \text{LUT}_C(\text{arg}_k^C)])) \quad (9)$$

where AFFORD is an affordance feature map (Section 4.1), LINEAR is a linear layer with bias, LUT_T and LUT_C are embedding lookup tables, and $[\cdot; \cdot]$ is a vector concatenation.

To sample a pose P , we first sample a position $(x, y) \sim P(x, y|g_k, \hat{s}_t)$, then sample a yaw angle $\omega_y \sim P(\omega_y|x, y; g_k, \hat{s}_t)$, and finally lookup a pitch angle $\omega_p = \mathbb{E}(\omega_p|x, y; g_k, \hat{s}_t)$.

A.3.4 InteractionMask

The InteractionMask procedure maps a state representation $\hat{s}_t = (V_t^S, V_t^O, v_t^S, P_t)$, the most recent RGB observation I_t , the most recent predicted segmentation I_t^S , and a subgoal $g_k = (\text{type}_k, \text{arg}_k^C, \text{arg}_k^M)$ to a 0-1 valued mask $\text{mask}_t \in [0, 1]^{H \times W}$ that identifies the interaction object in the first-person view observation. The interaction mask mask_t is in the format expected by ALFRED. Formally, it is computed in three steps:

$$\text{mask}_t^A = [I_t^S]_{\text{arg}_k^C} \quad (10)$$

$$\text{mask}_t^B = \text{PINHOLECAM}(\text{arg}_k^M, P_t) \quad (11)$$

$$\text{mask}_t = \text{mask}_t^A \cdot \text{mask}_t^B \quad (12)$$

where PINHOLECAM projects the 0-1 valued 3D voxel map arg_k^M to the agent's camera plane according to the pose P_t . The mask mask_t^A is an egocentric 0-1 valued mask that identifies all objects of class arg_k^C in the image I_t . The mask mask_t^B is an egocentric 0-1 valued mask that identifies the voxels arg_k^M . For each pixel (u, v) , the value $[\text{mask}_t^B]_{(u, v)}$ is the maximum of all values $[\text{arg}_k^M]_{(x, y, z)}$ over voxels with coordinates (x, y, z) that the ray cast from the camera through the pixel (u, v) intersects with. The final mask mask_t is a 0-1 valued mask that identifies not only the correct object class, but also the correct instance according to the voxel mask arg_k^M .

A.4 Additional Learning Details

A.4.1 Observation Model Learning

Data As described in Section 5, we use a perception dataset \mathcal{D}^P for training depth and segmentation models. The dataset $\mathcal{D}^P = \{([I]^{(i)}, [I^D]^{(i)}, [I^S]^{(i)})\}_{i=1}^{N_P}$ includes RGB images $[I]^{(i)}$ with ground truth depth $[I^D]^{(i)}$ and segmentation $[I^S]^{(i)}$. The ground truth depth $[I^D]^{(i)}$ at each pixel (u, v) is a distribution $[I^D]_{(u, v)}^{(i)}$ over B depth bins, where 100% of the probability mass is assigned to the bin containing the reference depth value. The ground truth segmentation $[I^S]^{(i)}$ is likewise at each pixel (u, v) a one-hot vector indicating the object class that pixel belongs to.

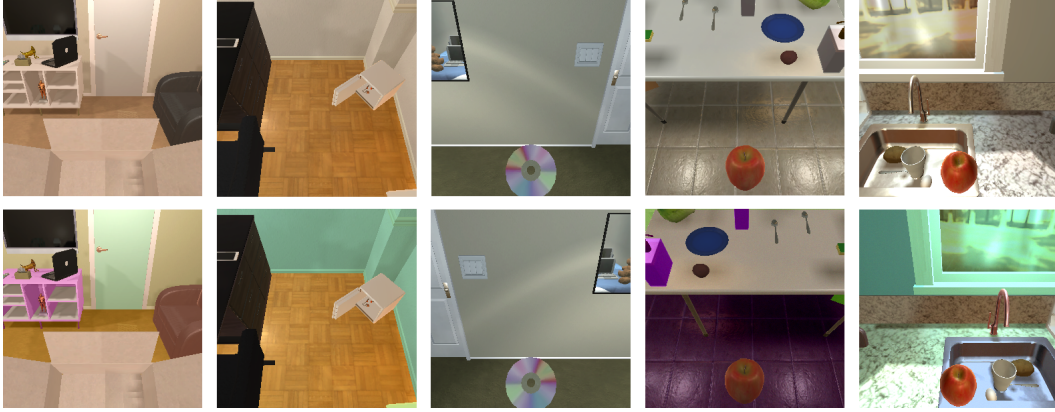


Figure 8: Examples of images produced with our AUGMENT procedure. The top row shows raw RGB images from ALFRED. The bottom row shows images generated by our segmentation-aware data augmentation method. Objects like walls, sinks, floors, and furniture randomly change color, while the apple and the spoons do not.

Data Augmentation The ALFRED dataset consists of 108 different training scenes, where each scene has a fixed furniture and light fixtures. Observations are highly correlated within each scene, which greatly reduces the effective size of the perception dataset and hurts generalization to unseen scenes. We use a custom segmentation-aware data augmentation strategy that increases the diversity of RGB observations.

We compute an augmented RGB image $\tilde{I} = \text{AUGMENT}(I, I^S, O_v)$ that maps the image I , ground-truth segmentation I^S , and a set of semantic classes O_v to a new image \tilde{I} . O_v is the set of object classes that are likely to appear in different colors. O_v includes classes like FLOOR, COUNTERTOP, CABINET, VASE, SOAPBOTTLE, ALARMCLOCK that come in different designs and colors, but not classes like BANANA, APPLE, SPOON that tend to have even appearance. Algorithm 1 shows the implementation of AUGMENT. It emulates more diverse environments by applying a different random color offset to each object class in the RGB image. Figure 8 shows examples of images produced with this augmentation procedure.

During training, we apply AUGMENT with 50% probability to each training example. Additionally, with 50% probability we perform a horizontal flip.

A.5 Additional Experimental Details

We collect a training dataset of language-demonstration pairs as described in Section 5. The demonstrations in ALFRED typically navigate while looking down at the floor, likely a side-effect of the PDDL planner that had access to the world state during data generation, and as such has no need to explore or observe the visual environment. We modify the demonstration trajectories to get more informative first-person observations. First, we insert four ROTATELEFT actions at the start of each trajectory. Second, we maintain a nominal camera pitch angle of 30° during navigation, by inserting LOOKDOWN and LOOKUP actions before and after every interaction action. We discard trajectories for which these modifications cause failures. These modifications result in observations that are more useful for learning and constructing our persistent spatial representation.

A.6 Hyperparameters

Table 5 shows hyperparameter values. The hyperparameters were hand-tuned on the validation unseen split.

A.7 Additional Results

Additional qualitative results are available at: <https://hlsm-alfred.github.io/>.

A successful example of task execution is available at: https://drive.google.com/file/d/1APKe3cR_-v1iyU2e1T5Un30w7PvkEdYs/view?usp=sharing

A failed example of task execution is available at: https://drive.google.com/file/d/1j8BJ_ALoXGyf8a-I0kmQAg38awSWYt6f/view?usp=sharing

Algorithm 1 AUGMENT

Input: RGB Image I , ground truth segmentation I^S , set of object classes O_v .

```
1:  $\tilde{I} \leftarrow I$ 
2: for  $c \in O_v$  do
3:    $\triangleright$  Extract a binary mask corresponding to object class  $c$ 
4:    $M_c \leftarrow [I^S]_{(c)}$ 
5:    $\triangleright$  Apply modifications to the image, masked by the segmentation mask  $M_c$ 
6:    $\triangleright \odot$  multiplies a  $N$ -dimensional vector with a  $H \times W$  tensor to compute a  $N \times H \times W$  tensor
7:    $\triangleright \cdot$  is an elementwise multiplication
8:   if randomBernoulli(0.5) then
9:      $\triangleright$  Sample an additive color offset for class  $c$  from a normal distribution.
10:     $\triangleright I_3$  is the  $3 \times 3$  identity matrix.
11:     $a \sim N(\vec{0}, \sigma_a I_3)$ 
12:     $\tilde{I} \leftarrow \tilde{I} + a \odot M_c$ 
13:   if randomBernoulli(0.5) then
14:      $\triangleright$  Sample additive gaussian noise for each pixel  $(u, v)$  for class  $c$ 
15:     for each pixel  $(u, v)$  do
16:        $g_{u,v} \sim N(1, \sigma_g)$ 
17:        $[\tilde{I}]_{(u,v)} \leftarrow [\tilde{I}]_{(u,v)} + g_{u,v} \cdot [M_c]_{(u,v)}$ 
18:   if randomBernoulli(0.5) then
19:      $\triangleright$  Sample an multiplicative color offset for class  $c$  from a normal distribution
20:      $m \sim N(\vec{0}, \sigma_m I_3)$ 
21:      $\tilde{I} \leftarrow \tilde{I} \cdot (m \odot M_c)$ 
22: clamp image  $\tilde{I}$  within 0-1 bounds
23: return  $\tilde{I}$ 
```

Hyperparameter	Value
Observation Model	
Number of depth bins B	50
Depth resolution ΔD	$0.1m$
Spatial State Representation	
Voxel Size	$0.25m$
Voxel Map Dimensions in Voxels	$61 \times 61 \times 10$
Voxel Map Dimensions in Meters	$15.25m \times 15.25m \times 2.5m$
Number of semantic classes C	123
High-level Controller	
Subgoal history encoder hidden dimension	128
Subgoal history encoder transformer layers	2
Subgoal predictor dense MLP layers	3
Subgoal predictor dense MLP hidden dimension	128
Low-level Controller	
Number of VIN iterations N^{vin}	122
VIN state space size	61×61
Development Environment	
Programming Language	Python
ML and Math Library	PyTorch

Table 5: Hyperparameter values.